Available online at www.sciencedirect.com
SCIENCE DIRECT®
ELSEVIER
International Journal of Solids and Structures 42 (2005) 6101–6121
INTERNATIONAL JOURNAL OF SOLIDS and STRUCTURES
www.elsevier.com/locate/ijsolstr

Postbuckling of FGM plates with piezoelectric actuators under thermo-electro-mechanical loadings

Hui-Shen Shen

School of Ocean and Civil Engineering, Shanghai Jiao Tong University, Shanghai 200030, PR China

Received 11 April 2004; received in revised form 11 March 2005
Available online 18 April 2005

Abstract

A postbuckling analysis is presented for a simply supported, shear deformable functionally graded plate with piezoelectric actuators subjected to the combined action of mechanical, electrical and thermal loads. The temperature field considered is assumed to be of uniform distribution over the plate surface and through the plate thickness and the electric field considered only has non-zero-valued component E_Z. The material properties of functionally graded materials (FGMs) are assumed to be graded in the thickness direction according to a simple power law distribution in terms of the volume fractions of the constituents, and the material properties of both FGM and piezoelectric layers are assumed to be temperature-dependent. The governing equations are based on a higher order shear deformation plate theory that includes thermo-piezoelectric effects. The initial geometric imperfection of the plate is taken into account. Two cases of the in-plane boundary conditions are considered. A two step perturbation technique is employed to determine buckling loads and postbuckling equilibrium paths. The numerical illustrations concern the postbuckling behavior of perfect and imperfect, geometrically mid-plane symmetric FGM plates with fully covered or embedded piezoelectric actuators under different sets of thermal and electric loading conditions. The effects played by temperature rise, volume fraction distribution, applied voltage, the character of in-plane boundary conditions, as well as initial geometric imperfections are studied.

Keywords: Hybrid laminated plate; Functionally graded materials; Temperature-dependent properties; Thermo-piezoelectric effect; Postbuckling

1. Introduction

Functionally graded materials (FGMs) are microscopically inhomogeneous composites usually made from a mixture of metals and ceramics. By gradually varying the volume fraction of constituent materials,

E-mail address: hsshen@mail.sjtu.edu.cn

0020-7683/$ - see front matter
doi:10.1016/j.ijsolstr.2005.03.042

their material properties exhibit a smooth and continuous change from one surface to another, thus eliminating interface problems and mitigating thermal stress concentrations. FGMs are now developed for general use as structural components in extremely high temperature environments. Another recent advance in material and structural engineering is in the field of smart structures which incorporates adaptive materials. Therefore, hybrid plate structures where a substrate made of FGMs is coupled with surface-bonded piezoelectric actuator and/or sensor layers have become increasingly important.

Many buckling studies for FGM plates subjected to mechanical or thermal loading are available in the literature, see, for example, Javaheri and Eslami (2002a,b,c), Najafizadeh and Eslami (2002a,b), Ma and Wang (2003a,b), and Wu (2004). It has been pointed out in Shen (2002), the governing differential equations for an FGM plate are identical in form to those of unsymmetric cross-ply laminated plates, and applying in-plane compressive loads to such plates will cause bending curvature to appear. Consequently, one wonders whether it is even possible to have a classical, bifurcation buckling problem for such FGM plates, and whether the existing solutions are really correct.

Leissa (1986), and Qatu and Leissa (1993) have proved that buckling may always occur for symmetric laminated plates with arbitrary in-plane loading and boundary conditions. It was also proved that for unsymmetric cross-ply laminated plates with all four edges simply supported the bifurcation buckling did not exist due to the stretching/bending coupling effect. Therefore, the buckling solutions obtained by Javaheri and Eslami (2002a,b,c) and Wu (2004) for simply supported FGM plates subjected to uniaxial compression and/or thermal loads may be incorrect.

Birman (1995) made the first attempt to solve the buckling problem of functionally graded hybrid composite plates. Feldman and Aboudi (1997) studied the buckling of composite plates with functionally graded distribution of reinforcement volume fraction. Note that in Birman (1995) and Feldman and Aboudi (1997) FGM has a different meaning, and they only investigated the mid-plane symmetric composite plates for which the stretching/bending coupling vanishes. Recently, Yang and Shen (2003) studied the postbuckling behavior of FGM thin plates under fully clamped boundary conditions. More recently, Liew et al. (2003) studied compressive postbuckling and thermal postbuckling behavior of FGM plates with two opposite edges clamped and with surface-bonded piezoelectric actuators. In Yang and Shen (2003) and Liew et al. (2003) they pointed out that the FGM plates with simply supported edges, even for the FGM hybrid plate which are not fully clamped, have no bifurcation solution.

The present paper extends the previous works (Shen, 2001, 2002) to the case of mid-plane symmetric FGM hybrid plates subjected to the combined action of mechanical, electrical and thermal loads. The temperature field considered is assumed to be of uniform distribution over the plate surface and through the plate thickness and the electric field considered only has non-zero-valued component E_Z. The material properties of FGMs are assumed to be graded in thickness direction according to a volume fraction power law distribution and expressed as a nonlinear function of temperature, whereas the material properties of piezoelectric layers are expressed as a linear function of temperature. The governing equations of the plate are based on Reddy's higher order shear deformation plate theory that includes thermo-piezoelectric effects (Reddy, 1999). All four edges of the plate are assumed to be simply supported, and two cases of the in-plane boundary conditions are considered. A two step perturbation technique is employed to determine buckling loads and postbuckling equilibrium paths. The initial geometric imperfection of the plate is taken into account but, for simplicity, its form is assumed to be the same as the initial buckling mode of the plate.

2. Theoretical development

We are now in a position to consider two types of hybrid laminated plate, referred to as $(\mathrm{P/FGM})_S$ and $(\mathrm{FGM/P})_S$, which consists of four plies and is mid-plane symmetric, as shown in Fig. 1. The length, width

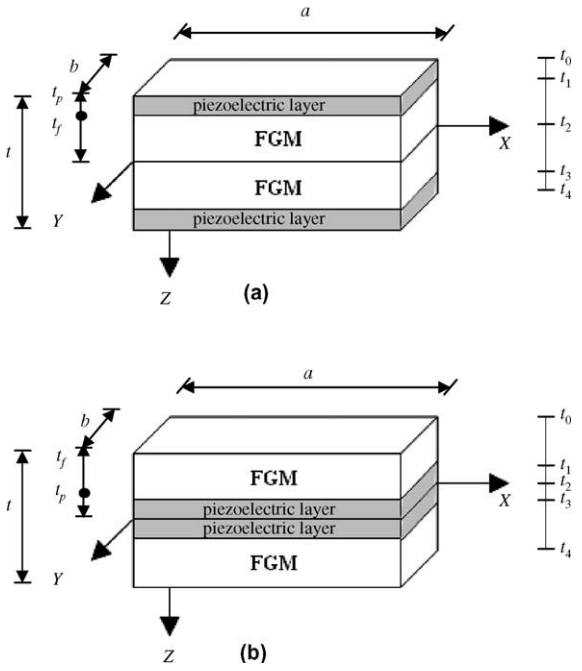

Fig. 1. Configurations of two types of hybrid laminated plates. (a) $(P/FGM)_S$ and (b) $(FGM/P)_S$ plate.

and total thickness of the hybrid laminated plate are a, b and t. The thickness of the FGM layer is t_f, while the thickness of the piezoelectric layer is t_p. The plate is assumed to be geometrically imperfect, and is subjected to a compressive edge load in the X-direction combined with thermal and electric loads. As usual, the coordinate system has its origin at the corner of the plate on the mid-plane. Let $\overline{U}$, $\overline{V}$ and $\overline{W}$ be the plate displacements parallel to a right-hand set of axes (X, Y, Z), where X is longitudinal and Z is perpendicular to the plate. $\overline{\Psi}_x$ and $\overline{\Psi}_y$ are the mid-plane rotations of the normals about the Y and X axes, respectively. Denoting the initial geometric imperfection by $\overline{W}^*(X,Y)$, let $\overline{W}(X,Y)$ be the additional deflection and $\overline{F}(X,Y)$ be the stress function for the stress resultants defined by $\overline{N}_x = \overline{F}_{,yy}$, $\overline{N}_y = \overline{F}_{,xx}$ and $\overline{N}_{xy} = -\overline{F}_{,xy}$, where a comma denotes partial differentiation with respect to the corresponding coordinates.

The substrate FGM layer is made from a mixture of ceramics and metals, the mixing ratio of which is varied continuously and smoothly in the Z direction, so that the effective material properties P_f (Young's modulus E_f or thermal expansion coefficient α_f) can be expressed as

$$P_f = P_c V_c + P_m V_m \tag{1}$$

where P_c and P_m denote the temperature-dependent properties of the ceramic and metal, respectively, and V_c and V_m are the ceramic and metal volume fractions and are related by

$$V_c + V_m = 1 \tag{2}$$

The volume fraction V_m follows a simple power law

$$V_m = \left(\frac{Z - t_1}{t_2 - t_1}\right)^N \tag{3}$$

where the volume fraction index N dictates the material variation profile through the FGM layer thickness.

It is assumed that the effective Young's modulus E_f and thermal expansion coefficient α_f of the FGM layer are of temperature-dependent, whereas Poisson's ratio v_f depends weakly on temperature change and is assumed to be a constant. From Eqs. (1)–(3), one has

$$E_f = (E_m - E_c)\left(\frac{Z - t_1}{t_2 - t_1}\right)^N + E_c, \quad \alpha_f = (\alpha_m - \alpha_c)\left(\frac{Z - t_1}{t_2 - t_1}\right)^N + \alpha_c \tag{4}$$

It is evident that when $Z = t_1$, $E_f = E_c$ and $\alpha_f = \alpha_c$, and when $Z = t_2$, $E_f = E_m$ and $\alpha_f = \alpha_m$. Furthermore, E_f and α_f are both temperature and position dependent.

Reddy (1984a,b) developed a simple higher order shear deformation plate theory, in which the transverse shear strains are assumed to be parabolically distributed across the plate thickness and which contains the same dependent unknowns as in the first-order shear deformation theory, and no shear correction factors are required. Based on Reddy's higher order shear deformation theory with a von Kármán-type of kinematic nonlinearity and including thermo-piezoelectric effects, the governing differential equations for an FGM plate with fully covered piezoelectric actuators can be derived in terms of a stress function $\overline{F}$, two rotations $\overline{\Psi}_x$ and $\overline{\Psi}_y$, and a transverse displacement $\overline{W}$, along with the initial geometric imperfection $\overline{W}^*$. They are

$$\widetilde{L}_{11}(\overline{W}) - \widetilde{L}_{12}(\overline{\Psi}_x) - \widetilde{L}_{13}(\overline{\Psi}_y) + \widetilde{L}_{14}(\overline{F}) - \widetilde{L}_{15}(\overline{N}^p) - \widetilde{L}_{16}(\overline{M}^p) = \widetilde{L}(\overline{W} + \overline{W}^*, \overline{F}) \tag{5}$$

$$\widetilde{L}_{21}(\overline{F}) + \widetilde{L}_{22}(\overline{\Psi}_x) + \widetilde{L}_{23}(\overline{\Psi}_y) - \widetilde{L}_{24}(\overline{W}) - \widetilde{L}_{25}(\overline{N}^p) = -\frac{1}{2}L(\overline{W} + 2\overline{W}^*, \overline{W}) \tag{6}$$

$$\widetilde{L}_{31}(\overline{W}) + \widetilde{L}_{32}(\overline{\Psi}_x) - \widetilde{L}_{33}(\overline{\Psi}_y) + \widetilde{L}_{34}(\overline{F}) - \widetilde{L}_{35}(\overline{N}^p) - \widetilde{L}_{36}(\overline{S}^p) = 0 \tag{7}$$

$$\widetilde{L}_{41}(\overline{W}) - \widetilde{L}_{42}(\overline{\Psi}_x) + \widetilde{L}_{43}(\overline{\Psi}_y) + \widetilde{L}_{44}(\overline{F}) - \widetilde{L}_{45}(\overline{N}^p) - \widetilde{L}_{46}(\overline{S}^p) = 0 \tag{8}$$

where

$$\begin{aligned}
\widetilde{L}_{15}(\overline{N}^p) &= \frac{\partial^2}{\partial X^2}(B_{11}^*\overline{N}_x^p + B_{21}^*\overline{N}_y^p) + 2\frac{\partial^2}{\partial X \partial Y}(B_{66}^*\overline{N}_{xy}^p) + \frac{\partial^2}{\partial Y^2}(B_{12}^*\overline{N}_x^p + B_{22}^*\overline{N}_y^p)\\
\widetilde{L}_{16}(\overline{M}^p) &= \frac{\partial^2}{\partial X^2}(\overline{M}_x^p) + 2\frac{\partial^2}{\partial X \partial Y}(\overline{M}_{xy}^p) + \frac{\partial^2}{\partial Y^2}(\overline{M}_y^p)\\
\widetilde{L}_{25}(\overline{N}^p) &= \frac{\partial^2}{\partial X^2}(A_{12}^*\overline{N}_x^p + A_{22}^*\overline{N}_y^p) - \frac{\partial^2}{\partial X \partial Y}(A_{66}^*\overline{N}_{xy}^p) + \frac{\partial^2}{\partial Y^2}(A_{11}^*\overline{N}_x^p + A_{12}^*\overline{N}_y^p)\\
\widetilde{L}_{35}(\overline{N}^p) &= \frac{\partial}{\partial X}\left[\left(B_{11}^* - \frac{4}{3t^2}E_{11}^*\right)\overline{N}_x^p + \left(B_{21}^* - \frac{4}{3t^2}E_{21}^*\right)\overline{N}_y^p\right] + \frac{\partial}{\partial Y}\left[\left(B_{66}^* - \frac{4}{3t^2}E_{66}^*\right)\overline{N}_{xy}^p\right]\\
\widetilde{L}_{36}(\overline{S}^p) &= \frac{\partial}{\partial X}(\overline{S}_x^p) + \frac{\partial}{\partial Y}(\overline{S}_{xy}^p)\\
\widetilde{L}_{45}(\overline{N}^p) &= \frac{\partial}{\partial X}\left[\left(B_{66}^* - \frac{4}{3t^2}E_{66}^*\right)\overline{N}_{xy}^p\right] + \frac{\partial}{\partial Y}\left[\left(B_{12}^* - \frac{4}{3t^2}E_{12}^*\right)\overline{N}_x^p + \left(B_{22}^* - \frac{4}{3t^2}E_{22}^*\right)\overline{N}_y^p\right]\\
\widetilde{L}_{46}(\overline{S}^p) &= \frac{\partial}{\partial X}(\overline{S}_{xy}^p) + \frac{\partial}{\partial Y}(\overline{S}_y^p)
\end{aligned} \tag{9}$$

and the other linear operators $\widetilde{L}_{ij}()$ and the nonlinear operator $\widetilde{L}()$ are defined as in Shen (2002).

In the above equations, the equivalent thermo-piezoelectric loads are defined by

$$\begin{bmatrix} \overline{N}^{\mathrm{P}} \\ \overline{M}^{\mathrm{P}} \\ \overline{P}^{\mathrm{P}} \end{bmatrix} = \begin{bmatrix} \overline{N}^{\mathrm{T}} \\ \overline{M}^{\mathrm{T}} \\ \overline{P}^{\mathrm{T}} \end{bmatrix} + \begin{bmatrix} \overline{N}^{\mathrm{E}} \\ \overline{M}^{\mathrm{E}} \\ \overline{P}^{\mathrm{E}} \end{bmatrix} \tag{10}$$

where $\overline{N}^{\mathrm{T}}, \overline{M}^{\mathrm{T}}, \overline{P}^{\mathrm{T}}$ and $\overline{N}^{\mathrm{E}}, \overline{M}^{\mathrm{E}}, \overline{P}^{\mathrm{E}}$ are the forces, moments and higher order moments caused by the elevated temperature and electric field, respectively.

The temperature field is assumed to be uniformly distributed over the plate surface and through the plate thickness.

For the plate type piezoelectric material, only the transverse direction electric field component E_Z is dominant, and E_Z is defined as $E_Z = -\Phi_{,Z}$, where Φ is the potential field. If the voltage applied to the actuator is in the thickness only, then

$$E_Z = \frac{V_k}{t_{\mathrm{p}}} \tag{11}$$

where V_k is the applied voltage across the kth ply.

The forces and moments caused by elevated temperature or electric field are defined by

$$\begin{bmatrix} \overline{N}_x^{\mathrm{T}} & \overline{M}_x^{\mathrm{T}} & \overline{P}_x^{\mathrm{T}} \\ \overline{N}_y^{\mathrm{T}} & \overline{M}_y^{\mathrm{T}} & \overline{P}_y^{\mathrm{T}} \\ \overline{N}_{xy}^{\mathrm{T}} & \overline{M}_{xy}^{\mathrm{T}} & \overline{P}_{xy}^{\mathrm{T}} \end{bmatrix} = \sum_{k=1} \int_{t_{k-1}}^{t_k} \begin{bmatrix} A_x \\ A_y \\ A_{xy} \end{bmatrix}_k (1, Z, Z^3) \Delta T \, \mathrm{d}Z \tag{12a}$$

$$\begin{bmatrix} \overline{S}_x^{\mathrm{T}} \\ \overline{S}_y^{\mathrm{T}} \\ \overline{S}_{xy}^{\mathrm{T}} \end{bmatrix} = \begin{bmatrix} \overline{M}_x^{\mathrm{T}} \\ \overline{M}_y^{\mathrm{T}} \\ \overline{M}_{xy}^{\mathrm{T}} \end{bmatrix} - \frac{4}{3t^2} \begin{bmatrix} \overline{P}_x^{\mathrm{T}} \\ \overline{P}_y^{\mathrm{T}} \\ \overline{P}_{xy}^{\mathrm{T}} \end{bmatrix} \tag{12b}$$

and

$$\begin{bmatrix} \overline{N}_x^{\mathrm{E}} & \overline{M}_x^{\mathrm{E}} & \overline{P}_x^{\mathrm{E}} \\ \overline{N}_y^{\mathrm{E}} & \overline{M}_y^{\mathrm{E}} & \overline{P}_y^{\mathrm{E}} \\ \overline{N}_{xy}^{\mathrm{E}} & \overline{M}_{xy}^{\mathrm{E}} & \overline{P}_{xy}^{\mathrm{E}} \end{bmatrix} = \sum_{k=1} \int_{t_{k-1}}^{t_k} \begin{bmatrix} B_x \\ B_y \\ B_{xy} \end{bmatrix}_k (1, Z, Z^3) \frac{V_k}{t_{\mathrm{p}}} \, \mathrm{d}Z \tag{12c}$$

$$\begin{bmatrix} \overline{S}_x^{\mathrm{E}} \\ \overline{S}_y^{\mathrm{E}} \\ \overline{S}_{xy}^{\mathrm{E}} \end{bmatrix} = \begin{bmatrix} \overline{M}_x^{\mathrm{E}} \\ \overline{M}_y^{\mathrm{E}} \\ \overline{M}_{xy}^{\mathrm{E}} \end{bmatrix} - \frac{4}{3t^2} \begin{bmatrix} \overline{P}_x^{\mathrm{E}} \\ \overline{P}_y^{\mathrm{E}} \\ \overline{P}_{xy}^{\mathrm{E}} \end{bmatrix} \tag{12d}$$

in which

$$\begin{bmatrix} A_x \\ A_y \\ A_{xy} \end{bmatrix} = - \begin{bmatrix} \overline{Q}_{11} & \overline{Q}_{12} & \overline{Q}_{16} \\ \overline{Q}_{12} & \overline{Q}_{22} & \overline{Q}_{26} \\ \overline{Q}_{16} & \overline{Q}_{26} & \overline{Q}_{66} \end{bmatrix} \begin{bmatrix} 1 & 0 \\ 0 & 1 \\ 0 & 0 \end{bmatrix} \begin{bmatrix} \alpha_{11} \\ \alpha_{22} \end{bmatrix} \tag{13a}$$

$$\begin{bmatrix} B_x \\ B_y \\ B_{xy} \end{bmatrix} = -\begin{bmatrix} \overline{Q}_{11} & \overline{Q}_{12} & \overline{Q}_{16} \\ \overline{Q}_{12} & \overline{Q}_{22} & \overline{Q}_{26} \\ \overline{Q}_{16} & \overline{Q}_{26} & \overline{Q}_{66} \end{bmatrix} \begin{bmatrix} 1 & 0 \\ 0 & 1 \\ 0 & 0 \end{bmatrix} \begin{bmatrix} d_{31} \\ d_{32} \end{bmatrix} \tag{13b}$$

where α_{11} and α_{22} are the thermal expansion coefficients measured in the longitudinal and transverse directions, respectively, d_{31} and d_{32} are the piezoelectric strain constants of a single ply, and $\overline{Q}_{ij}$ are the transformed elastic constants, details of which can be found in Reddy (1984a,b). Note that for an FGM layer, $\alpha_{11} = \alpha_{22} = \alpha_f$ is given in detail in Eq. (4), and $\overline{Q}_{ij} = Q_{ij}$ in which

$$Q_{11} = Q_{22} = \frac{E_f}{1 - \nu_f^2}, \quad Q_{12} = \frac{\nu_f E_f}{1 - \nu_f^2}, \quad Q_{16} = Q_{26} = 0, \quad Q_{66} = \frac{E_f}{2(1 + \nu_f)} \tag{14}$$

where E_f is also given in detail in Eq. (4), and varies in the thickness direction.

All four edges are assumed to be simply supported. Depending upon the in-plane behavior at the edges, two cases, Case 1 (referred to herein as movable edges) and Case 2 (referred to herein as immovable edges), will be considered. These correspond to the case when the motion of the unloaded edges in the plane tangent to the plate structure's mid-surface, normal to the respective edge is either unrestrained or completely restrained, respectively. As a result, we have

Case (1): The edges are simply supported and freely movable in the in-plane directions. In addition the plate is subjected to uniaxial compressive edge loads.

Case (2): All four edges are simply supported. Uniaxial edge loads are acting in the X-direction. The edges $X = 0, a$ are considered freely movable (in the in-plane direction), the remaining two edges being unloaded and immovable (i.e. prevented from moving in the Y-direction).

For both cases the associated boundary conditions could be found in Librescu and Stein (1991) and Shen and Zhang (1988). In the present paper, they are

$X = 0, a$:

$$\overline{W} = \overline{\Psi}_y = 0 \tag{15a}$$

$$\overline{N}_{xy} = 0, \quad \overline{M}_x = \overline{P}_x = 0 \tag{15b}$$

$$\int_0^b \overline{N}_x \, \mathrm{d}Y + P = 0 \tag{15c}$$

$Y = 0, b$:

$$\overline{W} = \overline{\Psi}_x = 0 \tag{15d}$$

$$\overline{N}_{xy} = 0, \quad \overline{M}_y = \overline{P}_y = 0 \tag{15e}$$

$$\int_0^a \overline{N}_y \, \mathrm{d}X = 0 \quad \text{(movable edges)} \tag{15f}$$

$$\overline{V} = 0 \quad \text{(immovable edges)} \tag{15g}$$

where P is a compressive edge load in the X-direction, $\overline{M}_x$ and $\overline{M}_y$ are the bending moments and $\overline{P}_x$ and $\overline{P}_y$ are the higher order moments as defined in Reddy (1984a,b).

Note that Eqs. (15c) and (15f) are satisfied in an average sense. As pointed out by Cui and Dowell (1983), two types of membrane boundary conditions, i.e. $\overline{N}_x$ and $\overline{N}_y$ in an average sense and point-wise along the boundary, do not have a strong influence on the buckling deflection.

The condition expressing the immovability condition $\overline{V}=0$ (on $Y=0,\ b$) is also fulfilled on the average sense as (Shen, 2001, 2002)

$$\int_0^a \int_0^b \frac{\partial \overline{V}}{\partial Y}\,\mathrm{d}Y\,\mathrm{d}X = 0 \tag{16}$$

This condition in conjunction with Eq. (17b) below provides the compressive stresses acting on the edges $Y=0,\ b$.

The average end-shortening relationships are

$$\begin{aligned}\frac{\Delta_x}{a} &= -\frac{1}{ab}\int_0^b\int_0^a \frac{\partial \overline{U}}{\partial X}\,\mathrm{d}X\,\mathrm{d}Y \\ &= -\frac{1}{ab}\int_0^b\int_0^a \left\{\left[A_{11}^*\frac{\partial^2\overline{F}}{\partial Y^2}+A_{12}^*\frac{\partial^2\overline{F}}{\partial X^2}+\left(B_{11}^*-\frac{4}{3t^2}E_{11}^*\right)\frac{\partial\overline{\Psi}_x}{\partial X}+\left(B_{12}^*-\frac{4}{3t^2}E_{12}^*\right)\frac{\partial\overline{\Psi}_y}{\partial Y}\right.\right. \\ &\quad \left.\left.-\frac{4}{3t^2}\left(E_{11}^*\frac{\partial^2\overline{W}}{\partial X^2}+E_{12}^*\frac{\partial^2\overline{W}}{\partial Y^2}\right)\right]-\frac{1}{2}\left(\frac{\partial\overline{W}}{\partial X}\right)^2-\frac{\partial\overline{W}}{\partial X}\frac{\partial\overline{W}^*}{\partial X}-(A_{11}^*\overline{N}_x^P+A_{12}^*\overline{N}_y^P)\right\}\mathrm{d}X\,\mathrm{d}Y\end{aligned} \tag{17a}$$

$$\begin{aligned}\frac{\Delta_y}{b} &= -\frac{1}{ab}\int_0^a\int_0^b \frac{\partial \overline{V}}{\partial Y}\,\mathrm{d}Y\,\mathrm{d}X \\ &= -\frac{1}{ab}\int_0^a\int_0^b \left\{\left[A_{22}^*\frac{\partial^2\overline{F}}{\partial X^2}+A_{12}^*\frac{\partial^2\overline{F}}{\partial Y^2}+\left(B_{21}^*-\frac{4}{3t^2}E_{21}^*\right)\frac{\partial\overline{\Psi}_x}{\partial X}+\left(B_{22}^*-\frac{4}{3t^2}E_{22}^*\right)\frac{\partial\overline{\Psi}_y}{\partial Y}\right.\right. \\ &\quad \left.\left.-\frac{4}{3t^2}\left(E_{21}^*\frac{\partial^2\overline{W}}{\partial X^2}+E_{22}^*\frac{\partial^2\overline{W}}{\partial Y^2}\right)\right]-\frac{1}{2}\left(\frac{\partial\overline{W}}{\partial Y}\right)^2-\frac{\partial\overline{W}}{\partial Y}\frac{\partial\overline{W}^*}{\partial Y}-(A_{12}^*\overline{N}_x^P+A_{22}^*\overline{N}_y^P)\right\}\mathrm{d}Y\,\mathrm{d}X\end{aligned} \tag{17b}$$

where Δ_x and Δ_y are plate end-shortening displacements in the X- and Y-directions.

In the above equations and what follows, the reduced stiffness matrices $[A_{ij}^*]$, $[B_{ij}^*]$, $[D_{ij}^*]$, $[E_{ij}^*]$, $[F_{ij}^*]$ and $[H_{ij}^*]$ $(i,j=1,2,6)$ are functions of temperature and position, determined through relationships (Shen, 2001, 2002)

$$\mathbf{A}^*=\mathbf{A}^{-1},\mathbf{B}^*=-\mathbf{A}^{-1}\mathbf{B},\mathbf{D}^*=\mathbf{D}-\mathbf{B}\mathbf{A}^{-1}\mathbf{B},\mathbf{E}^*=-\mathbf{A}^{-1}\mathbf{E},\mathbf{F}^*=\mathbf{F}-\mathbf{E}\mathbf{A}^{-1}\mathbf{B},\mathbf{H}^*=\mathbf{H}-\mathbf{E}\mathbf{A}^{-1}\mathbf{E} \tag{18a}$$

where A_{ij},B_{ij} etc., are the plate stiffnesses, defined by

$$(A_{ij},B_{ij},D_{ij},E_{ij},F_{ij},H_{ij})=\sum_{k=1}\int_{t_{k-1}}^{t_k}(\overline{Q}_{ij})_k(1,Z,Z^2,Z^3,Z^4,Z^6)\mathrm{d}Z\quad(i,j=1,2,6) \tag{18b}$$

It is evident that the above equations involve the stretching/bending coupling, as predicted by B_{ij} and E_{ij}. As argued previously, even for an FGM plate with all four edges simply supported, no bifurcation buckling could occur. For this reason, we consider here geometrically mid-plane symmetric FGM plates with fully covered or embedded piezoelectric actuators. In such a case, the stretching/bending coupling is zero-valued, i.e. $B_{ij}=E_{ij}=0$. As a result, $\widetilde{L}_{14}=\widetilde{L}_{15}=\widetilde{L}_{22}=\widetilde{L}_{23}=\widetilde{L}_{24}=\widetilde{L}_{34}=\widetilde{L}_{35}=\widetilde{L}_{44}=\widetilde{L}_{45}=0$.

3. Analytical method and asymptotic solutions

Having developed the theory, we will try to solve Eqs. (5)–(8) with boundary condition (15). Before proceeding, it is convenient first to define the following dimensionless quantities (with γ_{ijk} in Eq. (25) below are defined as in Shen (2002))

$$
\begin{aligned}
&x = \pi X/a, \quad y = \pi Y/b, \quad \beta = a/b, \quad (W, W^*) = (\overline{W}, \overline{W}^*)/[D_{11}^* D_{22}^* A_{11}^* A_{22}^*]^{1/4}\\
&F = \overline{F}/[D_{11}^* D_{22}^*]^{1/2}, \quad (\Psi_x, \Psi_y) = (\overline{\Psi}_x, \overline{\Psi}_y) a/\pi [D_{11}^* D_{22}^* A_{11}^* A_{22}^*]^{1/4}\\
&\gamma_{14} = [D_{22}^*/D_{11}^*]^{1/2}, \quad \gamma_{24} = [A_{11}^*/A_{22}^*]^{1/2}, \quad \gamma_5 = -A_{12}^*/A_{22}^*,\\
&(\gamma_{31}, \gamma_{41}) = (a^2/\pi^2)\left[A_{55} - 8D_{55}/t^2 + 16F_{55}/t^4, A_{44} - 8D_{44}/t^2 + 16F_{44}/t^4\right]/D_{11}^*,\\
&(\gamma_{T1}, \gamma_{T2}, \gamma_{P1}, \gamma_{P2}) = (A_x^{\mathrm{T}}, A_y^{\mathrm{T}}, B_x^P, B_y^P) a^2/\pi^2 [D_{11}^* D_{22}^*]^{1/2},\\
&(M_x, M_y, P_x, P_y) = (\overline{M}_x, \overline{M}_y, 4\overline{P}_x/3t^2, 4\overline{P}_y/3t^2) a^2/\pi^2 D_{11}^* [D_{11}^* D_{22}^* A_{11}^* A_{22}^*]^{1/4}\\
&(\delta_x, \delta_y) = (\Delta_x/a, \Delta_y/b) b^2/4\pi^2 [D_{11}^* D_{22}^* A_{11}^* A_{22}^*]^{1/2}, \quad \lambda_x = Pb/4\pi^2 [D_{11}^* D_{22}^*]^{1/2}
\end{aligned}
\tag{19}
$$

Also let

$$
\begin{bmatrix} A_x^{\mathrm{T}} \\ A_y^{\mathrm{T}} \end{bmatrix} \Delta T = -\sum_{k=1} \int_{t_{k-1}}^{t_k} \begin{bmatrix} A_x \\ A_y \end{bmatrix}_k \Delta T \, \mathrm{d}Z \tag{20a}
$$

$$
\begin{bmatrix} B_x^P \\ B_y^P \end{bmatrix} \Delta V = -\sum_{k=1} \int_{t_{k-1}}^{t_k} \begin{bmatrix} B_x \\ B_y \end{bmatrix}_k \frac{V_k}{t_{\mathrm{p}}} \, \mathrm{d}Z \tag{20b}
$$

The nonlinear Eqs. (5)–(8) may then be written in dimensionless form as

$$
L_{11}(W) - L_{12}(\Psi_x) - L_{13}(\Psi_y) = \gamma_{14}\beta^2 L(W + W^*, F) \tag{21}
$$

$$
L_{21}(F) = -\frac{1}{2}\gamma_{24}\beta^2 L(W + 2W^*, W) \tag{22}
$$

$$
L_{31}(W) + L_{32}(\Psi_x) - L_{33}(\Psi_y) = 0 \tag{23}
$$

$$
L_{41}(W) - L_{42}(\Psi_x) + L_{43}(\Psi_y) = 0 \tag{24}
$$

where

$$
\begin{aligned}
L_{11}() &= \gamma_{110}\frac{\partial^4}{\partial x^4} + 2\gamma_{112}\beta^2 \frac{\partial^4}{\partial x^2 \partial y^2} + \gamma_{114}\beta^4 \frac{\partial^4}{\partial y^4}\\
L_{12}() &= \gamma_{120}\frac{\partial^3}{\partial x^3} + \gamma_{122}\beta^2 \frac{\partial^3}{\partial x \partial y^2}\\
L_{13}() &= \gamma_{131}\beta\frac{\partial^3}{\partial x^2 \partial y} + \gamma_{133}\beta^3 \frac{\partial^3}{\partial y^3}\\
L_{21}() &= \frac{\partial^4}{\partial x^4} + 2\gamma_{212}\beta^2 \frac{\partial^4}{\partial x^2 \partial y^2} + \gamma_{214}\beta^4 \frac{\partial^4}{\partial y^4}\\
L_{31}() &= \gamma_{31}\frac{\partial}{\partial x} + \gamma_{310}\frac{\partial^3}{\partial x^3} + \gamma_{312}\beta^2 \frac{\partial^3}{\partial x \partial y^2}
\end{aligned}
$$

$$L_{32}() = \gamma_{31} - \gamma_{320}\frac{\partial^2}{\partial x^2} - \gamma_{322}\beta^2\frac{\partial^2}{\partial y^2}$$

$$L_{33}() = \gamma_{331}\beta\frac{\partial^2}{\partial x\partial y}$$

$$L_{41}() = \gamma_{41}\beta\frac{\partial}{\partial y} + \gamma_{411}\beta\frac{\partial^3}{\partial x^2\partial y} + \gamma_{413}\beta^3\frac{\partial^3}{\partial y^3}$$

$$L_{42}() = L_{33}()$$

$$L_{43}() = \gamma_{41} - \gamma_{430}\frac{\partial^2}{\partial x^2} - \gamma_{432}\beta^2\frac{\partial^2}{\partial y^2}$$

$$L() = \frac{\partial^2}{\partial x^2}\frac{\partial^2}{\partial y^2} - 2\frac{\partial^2}{\partial x\partial y}\frac{\partial^2}{\partial x\partial y} + \frac{\partial^2}{\partial y^2}\frac{\partial^2}{\partial x^2} \tag{25}$$

The boundary conditions expressed by Eq. (15) become

$x = 0,\ \pi$:

$$W = \Psi_y = 0 \tag{26a}$$

$$F_{,xy} = M_x = P_x = 0 \tag{26b}$$

$$\frac{1}{\pi}\int_0^\pi \beta^2\frac{\partial^2 F}{\partial y^2}\mathrm{d}y + 4\lambda_x\beta^2 = 0 \tag{26c}$$

$y = 0,\ \pi$:

$$W = \Psi_x = 0 \tag{26d}$$

$$F_{,xy} = M_y = P_y = 0 \tag{26e}$$

$$\int_0^\pi \frac{\partial^2 F}{\partial x^2}\mathrm{d}x = 0 \quad \text{(movable edges)} \tag{26f}$$

$$\delta_y = 0 \quad \text{(immovable edges)} \tag{26g}$$

and the unit end-shortening relationships become

$$\delta_x = -\frac{1}{4\pi^2\beta^2\gamma_{24}}\int_0^\pi\int_0^\pi \left\{\left[\gamma_{24}^2\beta^2\frac{\partial^2 F}{\partial y^2} - \gamma_5\frac{\partial^2 F}{\partial x^2} - \frac{1}{2}\gamma_{24}\left(\frac{\partial W}{\partial x}\right)^2 - \gamma_{24}\frac{\partial W}{\partial x}\frac{\partial W^*}{\partial x}\right] + (\gamma_{24}^2\gamma_{T1} - \gamma_5\gamma_{T2})\Delta T + (\gamma_{24}^2\gamma_{P1} - \gamma_5\gamma_{P2})\Delta V\right\}\mathrm{d}x\,\mathrm{d}y \tag{27a}$$

$$\delta_y = -\frac{1}{4\pi^2\beta^2\gamma_{24}}\int_0^\pi\int_0^\pi \left\{\left[\frac{\partial^2 F}{\partial x^2} - \gamma_5\beta^2\frac{\partial^2 F}{\partial y^2} - \frac{1}{2}\gamma_{24}\beta^2\left(\frac{\partial W}{\partial y}\right)^2 - \gamma_{24}\beta^2\frac{\partial W}{\partial y}\frac{\partial W^*}{\partial y}\right] + (\gamma_{T2} - \gamma_5\gamma_{T1})\Delta T + (\gamma_{P2} - \gamma_5\gamma_{P1})\Delta V\right\}\mathrm{d}y\,\mathrm{d}x \tag{27b}$$

It is noted that Eqs. (21)–(24) are identical in form to those of symmetric cross-ply laminated plates under mechanical loading. By virtue of the fact that ΔV and ΔT are assumed to be uniform, the thermo-piezoelectric coupling in Eqs. (5)–(8) vanishes, but terms in ΔV and ΔT intervene in Eq. (27).

Applying Eqs. (21)–(27), the compressive postbuckling behavior of perfect and imperfect, FGM hybrid plates with piezoelectric actuators under thermo-electro-mechanical loadings is now determined by means of a two step perturbation technique, for which the small perturbation parameter has no physical meaning at the first step, and is then replaced by a dimensionless deflection at the second step. The essence of this procedure, in the present case, is to assume that

$$\begin{aligned} W(x,y,\varepsilon) &= \sum_{j=1} \varepsilon^j w_j(x,y), \quad F(x,y,\varepsilon) = \sum_{j=0} \varepsilon^j f_j(x,y), \\ \Psi_x(x,y,\varepsilon) &= \sum_{j=1} \varepsilon^j \psi_{xj}(x,y), \quad \Psi_y(x,y,\varepsilon) = \sum_{j=1} \varepsilon^j \psi_{yj}(x,y) \end{aligned} \tag{28}$$

where ε is a small perturbation parameter and the first term of $w_j(x, y)$ is assumed to have the form

$$w_1(x,y) = A_{11}^{(1)} \sin mx \sin ny \tag{29}$$

and the initial geometric imperfection is assumed to have a similar form

$$W^*(x,y,\varepsilon) = \varepsilon a_{11}^* \sin mx \sin ny = \varepsilon\mu A_{11}^{(1)} \sin mx \sin ny \tag{30}$$

where $\mu = a_{11}^*/A_{11}^{(1)}$ is the imperfection parameter.

Substituting Eq. (28) into Eqs. (21)–(24) and collecting the terms of the same order of ε, a set of perturbation equations is obtained. By using Eqs. (29) and (30) to solve these perturbation equations of each order, the amplitudes of the terms $w_j(x,y)$, $f_j(x,y)$, $\psi_{xj}(x,y)$ and $\psi_{yj}(x,y)$ are determined step by step. As a result, up to fourth-order asymptotic solutions can be obtained.

$$W = \varepsilon[A_{11}^{(1)} \sin mx \sin ny] + \varepsilon^3[A_{13}^{(3)} \sin mx \sin 3ny + A_{31}^{(3)} \sin 3mx \sin ny] + \mathrm{O}(\varepsilon^5) \tag{31}$$

$$\begin{aligned} F = &- B_{00}^{(0)} \frac{y^2}{2} - b_{00}^{(0)} \frac{x^2}{2} + \varepsilon^2 \left[-B_{00}^{(2)} \frac{y^2}{2} - b_{00}^{(2)} \frac{x^2}{2} + B_{20}^{(2)} \cos 2mx + B_{02}^{(2)} \cos 2ny \right] \\ &+ \varepsilon^4 \left[-B_{00}^{(4)} \frac{y^2}{2} - b_{00}^{(4)} \frac{x^2}{2} + B_{20}^{(4)} \cos 2mx + B_{02}^{(4)} \cos 2ny + B_{22}^{(4)} \cos 2mx \cos 2ny + B_{40}^{(4)} \cos 4mx \right. \\ &\left. + B_{04}^{(4)} \cos 4ny + B_{24}^{(4)} \cos 2mx \cos 4ny + B_{42}^{(4)} \cos 4mx \cos 2ny \right] + \mathrm{O}(\varepsilon^5) \end{aligned} \tag{32}$$

$$\Psi_x = \varepsilon[C_{11}^{(1)} \cos mx \sin ny] + \varepsilon^3[C_{13}^{(3)} \cos mx \sin 3ny + C_{31}^{(3)} \cos 3mx \sin ny] + \mathrm{O}(\varepsilon^5) \tag{33}$$

$$\Psi_y = \varepsilon[D_{11}^{(1)} \sin mx \cos ny] + \varepsilon^3[D_{13}^{(3)} \sin mx \cos 3ny + D_{31}^{(3)} \sin 3mx \cos ny] + \mathrm{O}(\varepsilon^5) \tag{34}$$

It is mentioned that all coefficients in Eqs. (31)–(34) are related and can be expressed in terms of $A_{11}^{(1)}$ but, for the sake of brevity, the detailed expressions are not shown.

Next, upon substitution of Eqs. (31)–(34) into the boundary conditions (26c) and (27a), the postbuckling equilibrium path can be written as

$$\lambda_x = \lambda_x^{(0)} + \lambda_x^{(2)} W_{\mathrm{m}}^2 + \lambda_x^{(4)} W_{\mathrm{m}}^4 + \cdots \tag{35}$$

and

$$\delta_x = \delta_x^{(0)} + \delta_x^{(2)} W_{\mathrm{m}}^2 + \delta_x^{(4)} W_{\mathrm{m}}^4 + \cdots \tag{36}$$

in which W_m is the dimensionless form of maximum deflection, which is assumed to be at the point $(x,y)=(\pi/2m,\pi/2n)$ and $\lambda_x^{(i)}$ and $\delta_x^{(i)}$ $(i=0,2,4,\ldots)$ are given in detail in Appendix A.

Eqs. (35) and (36) can be employed to obtain numerical results for the postbuckling load–deflection or load-end-shortening curves of simply supported shear deformable FGM plates with piezoelectric actuators subjected to uniaxial compression combined with thermal and electric loads. From Appendix A, the buckling load of a perfect plate can readily be obtained numerically, by setting $\mu=0$ (or $\overline{W}^*/t=0$), while taking $W_m=0$ (or $\overline{W}/t=0$). In such a case, the minimum buckling load is determined by applying Eq. (35) for various values of the buckling mode (m,n), which determine the number of half-waves in the X- and Y-directions.

4. Numerical results and discussions

To study the thermo-piezoelectric effects on the postbuckling behavior of FGM hybrid plates under uniaxial compression, several numerical examples were solved for perfect and imperfect, $(P/FGM)_S$ and $(FGM/P)_S$ plates. Two sets of material mixture for FGMs are considered. One is silicon nitride and stainless steel, referred to as Si_3N_4/SUS304, and the other is zirconium oxide and titanium alloy, referred to as ZrO_2/Ti–6Al–4V. However, the analysis is equally applicable to other types of FGMs as well. The material properties P_f, such as Young's modulus E_f and thermal expansion coefficient α_f, can be expressed as a nonlinear function of temperature as (Touloukian, 1967)

$$P_f = P_0(P_{-1}T^{-1}+1+P_1T+P_2T^2+P_3T^3) \tag{37}$$

in which $T=T_0+\Delta T$, and $T_0=300$ K. P_0, P_{-1}, P_1, P_2 and P_3 are the coefficients of temperature T (K) and are unique to the constituent materials. Typical values for Young's modulus E_f (in Pa) and thermal expansion coefficient α_f (in/K) of these materials are listed in Table 1 (from Reddy and Chin, 1998). Poisson's ratio v_f is assumed to be a constant, and $v_f=0.28$. PZT-5A is selected for the piezoelectric layers. The material properties of which are assumed to be linear functions of temperature change, i.e.

$$\begin{aligned}
&E_{11}(T)=E_{110}(1+E_{111}\Delta T), \quad E_{22}(T)=E_{220}(1+E_{221}\Delta T)\\
&G_{12}(T)=G_{120}(1+G_{121}\Delta T), \quad G_{13}(T)=G_{130}(1+G_{131}\Delta T), \quad G_{23}(T)=G_{230}(1+G_{231}\Delta T)\\
&\alpha_{11}(T)=\alpha_{110}(1+\alpha_{111}\Delta T), \quad \alpha_{22}(T)=\alpha_{220}(1+\alpha_{221}\Delta T)
\end{aligned} \tag{38}$$

where E_{110}, E_{220}, G_{120}, G_{130}, G_{230}, α_{110}, α_{220}, E_{111}, E_{221}, G_{121}, G_{131}, G_{231}, α_{111}, α_{221} are constants. Typical values adopted, as given in Oh et al. (2000), $E_{110}=E_{220}=61$ GPa, $G_{120}=G_{130}=G_{230}=24.2$ GPa,

Table 1
Temperature-dependent coefficients for ceramics and metals, from Reddy and Chin (1998)

Materials		P_0	P_{-1}	P_1	P_2	P_3
Zirconia	E_f	244.27e+9	0	−1.371e−3	1.214e−6	−3.681e−10
	α_f	12.766e−6	0	−1.491e−3	1.006e−5	−6.778e−11
Silicon nitride	E_f	348.43e+9	0	−3.070e−4	2.160e−7	−8.946e−11
	α_f	5.8723e−6	0	9.095e−4	0	0
Ti–6Al–4V	E_f	122.56e+9	0	−4.586e−4	0	0
	α_f	7.5788e−6	0	6.638e−4	−3.147e−6	0
Stainless steel	E_f	201.04e+9	0	3.079e−4	−6.534e−7	0
	α_f	12.330e−6	0	8.086e−4	0	0

$v_{12} = 0.3$, $\alpha_{110} = \alpha_{220} = 0.9 \times 10^{-6}/\mathrm{K}$ and $d_{31} = d_{32} = 2.54 \times 10^{-10}$ m/V; and $E_{111} = -0.0005$, $E_{221} = G_{121} = G_{131} = G_{231} = -0.0002$, $\alpha_{111} = \alpha_{221} = 0.0005$.

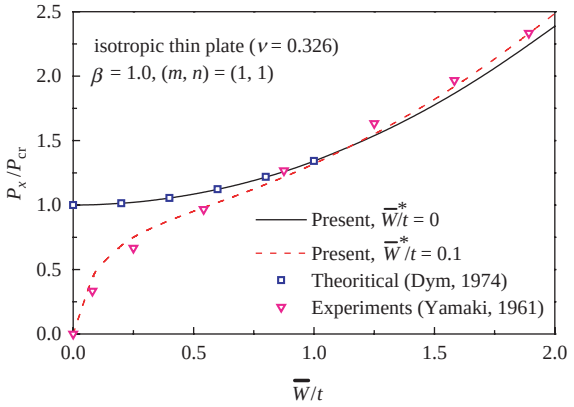

Fig. 2. Comparisons of postbuckling load–deflection curves for isotropic thin plates under uniaxial compression.

Table 2
Comparisons of buckling loads P_{cr} (kN) for uniaxial compressed, $(P/FGM)_S$ plates with a substrate made of Si_3N_4/SUS304 and with unloaded edges immovable under uniform temperature rise and three sets of electrical loading conditions ($b/t = 20$, $a/b = 1.0$, $T_0 = 300$ K)

ΔT	$V_U = V_L$	$N = 0$	$N = 0.2$	$N = 0.5$	$N = 1.0$	$N = 2.0$	$N = 5.0$
$(P/FGM)_S$, TID, $(m, n) = (1,1)$							
0 K	−500 V	115.2026	131.6953	146.1075	157.9360	166.5642	171.3940
	0 V	114.6376	131.1302	145.5423	157.3708	165.9990	170.8288
	+500 V	114.0725	130.5651	144.9771	156.8056	165.4337	170.2635
100 K	−500 V	93.3042	109.9468	124.9499	137.6636	147.3829	153.4537
	0 V	92.7391	109.3817	124.3848	137.0984	146.8177	152.8885
	+500 V	92.1741	108.8166	123.8196	136.5332	146.2524	152.3232
200 K	−500 V	71.4058	88.1983	103.7924	117.3912	128.2016	135.5134
	0 V	70.8407	87.6332	103.2272	116.8260	127.6364	134.9482
	+500 V	70.2757	87.0681	102.6621	116.2608	127.0711	134.3829
$(P/FGM)_S$, TD-F, $(m, n) = (1,1)$							
100 K	−500 V	90.7119	106.8642	121.4538	133.8422	143.3414	149.3148
	0 V	90.1468	106.2991	120.8886	133.2770	142.7762	148.7495
	+500 V	89.5818	105.7340	120.3235	132.7118	142.2110	148.1842
200 K	−500 V	63.4408	79.6302	94.7616	108.0310	118.6513	125.9229
	0 V	62.8758	79.0652	94.1965	107.4658	118.0861	125.3576
	+500 V	62.3107	78.5001	93.6314	106.9006	117.5209	124.7924
$(P/FGM)_S$, TD, $(m, n) = (1,1)$							
100 K	−500 V	90.4283	106.5790	121.1672	133.5544	143.0529	149.0257
	0 V	89.8680	106.0187	120.6067	132.9939	142.4923	148.4651
	+500 V	89.3077	105.4583	120.0463	132.4334	141.9318	147.9045
200 K	−500 V	62.8991	79.0828	94.2088	107.4735	118.0899	125.3583
	0 V	62.3435	78.5270	93.6530	106.9176	117.5339	124.8023
	+500 V	61.7878	77.9712	93.0971	106.3616	116.9779	124.2462

The accuracy and effectiveness of the present method for the buckling and postbuckling analyses of isotropic and/or symmetric cross-ply laminated plates subjected to uniaxial compression were examined by many comparison studies given in Shen (1998, 2000a,b,c, 2001) and Shen and Zhang (1988). In addition, the postbuckling load–deflection curves for perfect and imperfect, isotropic thin square plates ($\nu = 0.326$) subjected to uniaxial compression are compared in Fig. 2 with the analytical solutions of Dym (1974) and the experimental results of Yamaki (1961). These comparisons show that the results from the present method are in good agreement with the existing results, thus verifying the reliability and accuracy of the present method.

A parametric study has been carried out and typical results are shown in Tables 2–7 and Figs. 3–8. For these examples, the plate geometric parameter $a/b = 1$, $b/t = 20$ and 40, and the thickness of the FGM layer $t_f = 1$ mm whereas the thickness of piezoelectric layers $t_p = 0.1$ mm, so that the total thickness of the plate $t = 2.2$ mm. It should be appreciated that in all figures $\overline{W}^*/t = 0.1$ denotes the dimensionless maximum initial geometric imperfection of the plate.

Tables 2–5 present the buckling loads P_{cr} (in kN) for perfect, moderately thick ($b/t = 20$), $(P/FGM)_S$ and $(FGM/P)_S$ hybrid laminated plates with unloaded edges immovable and with different values of the volume fraction index N (=0.0, 0.2, 0.5, 1.0, 2.0 and 5.0) subjected to uniaxial compression under three sets of temperature rise ($\Delta T = 0$, 100, 200 K). Here, TD represents material properties for both substrate FGM layer

Table 3
Comparisons of buckling loads P_{cr} (kN) for uniaxial compressed, $(FGM/P)_S$ plates with a substrate made of Si_3N_4/SUS304 and with unloaded edges immovable under uniform temperature rise and three sets of electrical loading conditions ($b/t = 20$, $a/b = 1.0$, $T_0 = 300$ K)

ΔT	V_M	$N = 0$	$N = 0.2$	$N = 0.5$	$N = 1.0$	$N = 2.0$	$N = 5.0$
$(FGM/P)_S$, TID, $(m, n) = (1,1)$							
0 K	−500 V	138.5191	159.3017	177.6971	193.1219	204.8333	212.0199
	0 V	137.9540	158.7366	177.1320	192.5568	204.2680	211.4547
	+500 V	137.3889	158.1714	176.5668	191.9915	203.7028	210.8894
100 K	−500 V	116.6206	137.5532	156.5396	172.8495	185.6520	194.0796
	0 V	116.0556	136.9881	155.9744	172.2843	185.0867	193.5144
	+500 V	115.4905	136.4229	155.4093	171.7191	184.5215	192.9491
200 K	−500 V	94.7222	115.8047	135.3821	152.5771	166.4707	176.1393
	0 V	94.1571	115.2396	134.8169	152.0119	165.9054	175.5741
	+500 V	93.5921	114.6745	134.2518	151.4467	165.3402	175.0088
$(FGM/P)_S$, TD-F, $(m, n) = (1,1)$							
100 K	−500 V	113.5414	133.8505	152.2997	168.1724	180.6583	188.9140
	0 V	112.9764	133.2854	151.7345	167.6072	180.0931	188.3488
	+500 V	112.4113	132.7203	151.1694	167.0420	179.5278	187.7835
200 K	−500 V	85.3580	105.6978	124.6823	141.4299	155.0314	164.5812
	0 V	84.7929	105.1327	124.1171	140.8647	154.4662	164.0159
	+500 V	84.2279	104.5676	123.5520	140.2995	153.9010	163.4507
$(FGM/P)_S$, TD, $(m, n) = (1,1)$							
100 K	−500 V	113.5180	133.8241	152.2709	168.1422	180.6273	188.8832
	0 V	112.9577	133.2637	151.7105	167.5817	180.0668	188.3226
	+500 V	112.3974	132.7033	151.1500	167.0212	179.5062	187.7620
200 K	−500 V	85.3354	105.6667	124.6441	141.3861	154.9840	164.5320
	0 V	84.7797	105.1109	124.0882	140.8302	154.4280	163.9759
	+500 V	84.2241	104.5552	123.5323	140.2742	153.8719	163.4198

and piezoelectric layers are temperature-dependent. TD-F represents material properties of substrate FGM layer are temperature-dependent but material properties of piezoelectric layers are temperature-independent, i.e. $E_{111} = E_{221} = G_{121} = G_{131} = G_{231} = \alpha_{111} = \alpha_{221} = 0$ in Eq. (38). TID represents material properties for both piezoelectric layers and substrate FGM layer are temperature-independent, i.e. in a fixed temperature $T_0 = 300$ K for FGM layer, as previously used in Yang and Shen (2003). The control voltages with the same sign are also applied to the upper, lower or middle piezoelectric layers, and are referred to as V_U, V_L and V_M. Three electrical loading cases are considered. Here $V_U = V_L = 0$ V (or $V_M = 0$ V) implies that the buckling occurs under a grounding condition. Two kinds of substrate FGM layers, i.e. Si_3N_4/SUS304 and ZrO_2/Ti–6Al–4V are considered. It can be found that the buckling load of $(P/FGM)_S$ plate is lower than that of $(FGM/P)_S$ plate. It can be seen that, for the hybrid plates with Si_3N_4/SUS304 substrate, a fully metallic plate ($N = 0$) has lowest buckling load and that the buckling load increases as the volume fraction index N increases. This is expected because the metallic plate has a lower stiffness than the ceramic plate. It is found that the increase is about +65% for the $(P/FGM)_S$ plate, and about +67% for the $(FGM/P)_S$ one, from $N = 0$ to $N = 5$, under temperature change $\Delta T = 100$ K. It can also be seen that the temperature reduces the buckling load when the temperature dependency is put into consideration. The percentage decrease is about −14% for the $(P/FGM)_S$ plate and about −12% for the $(FGM/P)_S$ one from temperature changes from $\Delta T = 0$ K to $\Delta T = 100$ K under the same volume fraction distribution $N = 2$.

Table 4
Comparisons of buckling loads P_{cr} (kN) for uniaxial compressed, $(P/FGM)_S$ plates with a substrate made of ZrO_2/Ti–6Al–4V and with unloaded edges immovable under uniform temperature rise and three sets of electrical loading conditions ($b/t = 20$, $a/b = 1.0$, $T_0 = 300$ K)

ΔT	$V_U = V_L$	$N = 0$	$N = 0.2$	$N = 0.5$	$N = 1.0$	$N = 2.0$	$N = 5.0$
$(P/FGM)_S$, TID, $(m, n) = (1, 1)$							
0 K	−500 V	64.0000	72.9739	80.8184	87.2604	91.9643	94.6043
	0 V	63.4356	72.4094	80.2538	86.6957	91.3996	94.0395
	+500 V	62.8712	71.8449	79.6892	86.1310	90.8348	93.4747
100 K	−500 V	57.5279	64.4956	70.0364	73.9762	76.0389	75.9364
	0 V	56.9635	63.9311	69.4718	73.4115	75.4741	75.3716
	+500 V	56.3991	63.3666	68.9072	72.8468	74.9094	74.8068
200 K	−500 V	51.0557	56.0172	59.2544	60.6920	60.1135	57.2686
	0 V	50.4913	55.4527	58.6898	60.1273	59.5487	56.7037
	+500 V	49.9269	54.8882	58.1252	59.5626	58.9839	56.1389
$(P/FGM)_S$, TD-F, $(m, n) = (1, 1)$							
100 K	−500 V	54.8204	59.5851	62.9913	64.9500	65.2654	63.7199
	0 V	54.2561	59.0207	62.4268	64.3854	64.7007	63.1551
	+500 V	53.6917	58.4563	61.8623	63.8208	64.1360	62.5904
200 K	−500 V	45.9786	45.1848	42.4283	37.8905	31.5562	23.3350
	0 V	45.4144	44.6205	41.8639	37.3260	30.9916	22.7704
	+500 V	44.8502	44.0561	41.2995	36.7615	30.4270	22.2057
$(P/FGM)_S$, TD, $(m, n) = (1, 1)$							
100 K	−500 V	54.5302	59.2967	62.7049	64.6657	64.9834	63.4404
	0 V	53.9709	58.7372	62.1453	64.1060	64.4237	62.8805
	+500 V	53.4117	58.1778	61.5857	63.5464	63.8639	62.3206
200 K	−500 V	45.4104	44.6291	41.8861	37.3619	31.0410	22.8328
	0 V	44.8561	44.0746	41.3314	36.8071	30.4860	22.2777
	+500 V	44.3018	43.5201	40.7768	36.2523	29.9311	21.7227

Also the buckling loads under TD-F and TD cases are very close under the same volume fraction distribution and the same temperature change. In contrast, for the ZrO_2/Ti–6Al–4V hybrid laminated plate, the buckling load is lower than that of the Si_3N_4/SUS304 hybrid laminated plate and erratic behavior can be observed in thermal loading conditions $\Delta T = 100$ K and 200 K. Therefore, only Si_3N_4/SUS304 hybrid laminated plate under TD case is considered in the postbuckling studies (in Figs. 3–8). It can also be seen that the control voltage has a very small effect on the buckling loads for hybrid laminated plates, this is because the piezoelectric layer is much thinner than the FGM substrate. Very high voltages will be able to influence the buckling response of the hybrid laminated plate. However, such high voltages cannot be applied, because they lead to a breakdown in the material properties.

Then Tables 6 and 7 present the buckling loads P_{cr} for the same two types of hybrid plates with unloaded edges movable subjected to uniaxial compression under three sets of temperature rise ($\Delta T = 0$, 100, 200 K). The results show that the buckling load is decreased with increase in temperature, but is increased as volume fraction index N increases at the same temperature. The numerical results also confirm that the control voltage has no effect on the buckling loads of hybrid laminated plates when the unloaded edges are movable.

Figs. 3 and 4 give, respectively, the postbuckling load–deflection and load–shortening curves for (P/FGM)$_S$ and (FGM/P)$_S$ hybrid laminated plates ($b/t = 40$, $N = 0.2$) with unloaded edges immovable

Table 5
Comparisons of buckling loads P_{cr} (kN) for uniaxial compressed, (FGM/P)$_S$ plates with a substrate made of ZrO_2/Ti–6Al–4V and with unloaded edges immovable under uniform temperature rise and three sets of electrical loading conditions ($b/t = 20$, $a/b = 1.0$, $T_0 = 300$ K)

ΔT	V_M	$N = 0$	$N = 0.2$	$N = 0.5$	$N = 1.0$	$N = 2.0$	$N = 5.0$
(FGM/P)$_S$, TID, $(m, n) = (1, 1)$							
0 K	−500 V	70.7813	82.1124	92.1400	100.5459	106.9247	110.8339
	0 V	70.2169	81.5479	91.5754	99.9812	106.3599	110.2691
	+500 V	69.6525	80.9834	91.0108	99.4165	105.7951	109.7042
100 K	−500 V	64.3091	73.6340	81.3580	87.2617	90.9992	92.1660
	0 V	63.7448	73.0695	80.7934	86.6970	90.4345	91.6012
	+500 V	63.1804	72.5050	80.2288	86.1323	89.8697	91.0364
200 K	−500 V	57.8370	65.1557	70.5760	73.9775	75.0738	73.4981
	0 V	57.2726	64.5912	70.0113	73.4128	74.5090	72.9333
	+500 V	56.7082	64.0267	69.4467	72.8481	73.9443	72.3685
(FGM/P)$_S$, TD-F, $(m, n) = (1, 1)$							
100 K	−500 V	60.6917	67.4217	72.6482	76.2438	77.9534	77.4619
	0 V	60.1274	66.8572	72.0837	75.6792	77.3888	76.8972
	+500 V	59.5631	66.2928	71.5192	75.1146	76.8241	76.3325
200 K	−500 V	50.9401	51.8613	50.6936	47.5837	42.4644	35.1598
	0 V	50.3759	51.2970	50.1292	47.0192	41.8998	34.5951
	+500 V	49.8116	50.7327	49.5647	46.4547	41.3352	34.0305
(FGM/P)$_S$, TD, $(m, n) = (1, 1)$							
100 K	−500 V	60.6634	67.3937	72.6214	76.2187	77.9306	77.4421
	0 V	60.1041	66.8343	72.0618	75.6590	77.3708	76.8822
	+500 V	59.5448	66.2749	71.5022	75.0993	76.8111	76.3223
200 K	−500 V	50.8947	51.8260	50.6700	47.5728	42.4668	35.1762
	0 V	50.3404	51.2715	50.1153	47.0180	41.9118	34.6211
	+500 V	49.7861	50.7170	49.5606	46.4632	41.3569	34.0661

subjected to uniaxial compression and three sets of electrical loading, $V_U = V_L$ (or V_M) $= -500, 0, +500$ V, and under $\Delta T = 0$ and 100 K. It is evident that the buckling loads reduce as the temperature increases, and the postbuckling path becomes lower. It can be found that the control voltage has a small effect on the postbuckling behavior of the plate. It can be seen that minus control voltages increase the buckling load and decrease the postbuckled deflection at the same temperature rise, whereas the plus control voltages decrease the buckling load and induce more large postbuckled deflections.

Figs. 5 and 6 show the effect of the volume fraction index N (=0.2, 1.0 and 5.0) on the postbuckling behavior of $(P/FGM)_S$ and $(FGM/P)_S$ hybrid laminated plates ($b/t = 40$) with unloaded edges immovable subjected to uniaxial compression and three sets of electrical loading, and under $\Delta T = 100$ K. It can be seen that the increase of the volume fraction index N yields an increase of the buckling load and postbuckling strength.

Table 6
Comparisons of buckling loads P_{cr} (kN) for uniaxial compressed, Si_3N_4/SUS304 plates with piezoelectric actuators and with unloaded edges movable subjected to temperature rise ($b/t = 20$, $a/b = 1.0$, $T_0 = 300$ K)

	ΔT (K)	$N = 0.0$	$N = 0.2$	$N = 0.5$	$N = 1.0$	$N = 2.0$	$N = 5.0$
$(P/FGM)_S$, $(m, n) = (1,1)$							
TID		146.8044	167.9184	186.3678	201.5086	212.5516	218.7312
TD-FGM	100	144.8755	165.3297	183.2028	197.8707	208.5686	214.5550
	200	141.2601	161.6779	179.5191	194.1613	204.8411	210.8181
TD	100	144.5326	164.9874	182.8609	197.5289	208.2266	214.2126
	200	140.5758	160.9947	178.8367	193.4790	204.1585	210.1347
$(FGM/P)_S$, $(m, n) = (1,1)$							
TID		176.6633	203.2696	226.8185	246.5632	261.5528	270.7491
TD-FGM	100	174.1111	199.8871	222.7014	241.8298	256.3509	265.2588
	200	169.3277	195.0592	217.8333	236.9282	251.4242	260.3173
TD	100	174.1070	199.8824	222.6962	341.8245	256.3456	265.2538
	200	169.3195	195.0497	217.8229	236.9173	251.4135	260.3075

Table 7
Comparisons of buckling loads P_{cr} (kN) for uniaxial compressed, ZrO_2/Ti–6Al–4V plates with piezoelectric actuators and with unloaded edges movable subjected to temperature rise temperature rise ($b/t = 20$, $a/b = 1.0$, $T_0 = 300$ K)

	ΔT (K)	$N = 0.0$	$N = 0.2$	$N = 0.5$	$N = 1.0$	$N = 2.0$	$N = 5.0$
$(P/FGM)_S$, $(m, n) = (1,1)$							
TID		81.2698	92.7595	102.8020	111.0477	117.0674	120.4437
TD-FGM	100	77.6612	87.2275	95.5896	102.4555	107.4673	110.2784
	200	74.0524	82.3901	89.6789	95.6635	100.0321	102.4828
TD	100	77.3189	86.8857	95.2482	102.1141	107.1257	109.9364
	200	73.3692	81.7080	88.9973	94.9821	99.3503	101.8001
$(FGM/P)_S$, $(m, n) = (1,1)$							
TID		89.9576	104.4662	117.3045	128.0650	136.2290	141.2302
TD-FGM	100	85.1835	97.2669	107.9604	116.9225	123.7195	127.8799
	200	80.4093	90.9440	100.2675	108.0808	114.0052	117.6293
TD	100	85.1797	97.2626	107.9557	116.9175	123.7146	127.8754
	200	80.4018	90.9355	100.2582	108.0712	113.9956	117.6204

Figs. 7 and 8 show the effect of temperature rise ΔT (=0, 100, and 200 K) on the postbuckling behavior of $(P/FGM)_S$ and $(FGM/P)_S$ hybrid laminated plates ($b/t = 40$) with unloaded edges movable and with $N = 0.2$ and 2.0 subjected to uniaxial compression. It can be seen that both buckling load and postbuckling strength are decreased with increase in temperature. It can also be seen that the buckling load of hybrid laminated plates with immovable unloaded edges is lower than that of the plate with movable unloaded edges under the same loading conditions, compare Figs. 3 and 7, and Figs. 4 and 8. In contrast, the postbuckling load carrying capacity of the plate with immovable unloaded edges is larger than that of the plate with movable unloaded edges when the deflection $\overline{W}$ is sufficiently large.

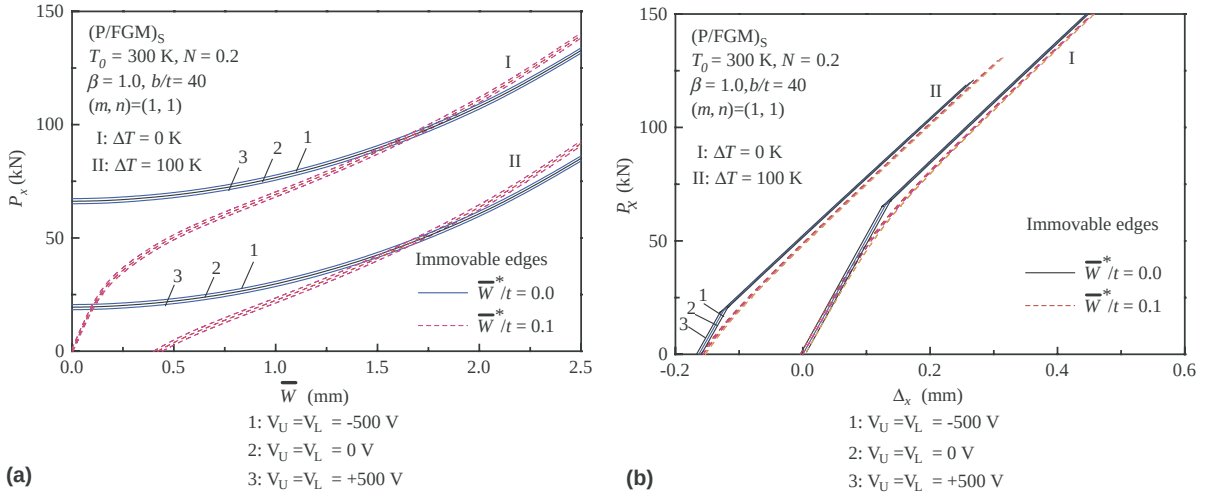

Fig. 3. Thermo-piezoelectric effects on the postbuckling behavior of $(P/FGM)_S$ plates with unload edges immovable. (a) Load–deflection (b) load–shortening.

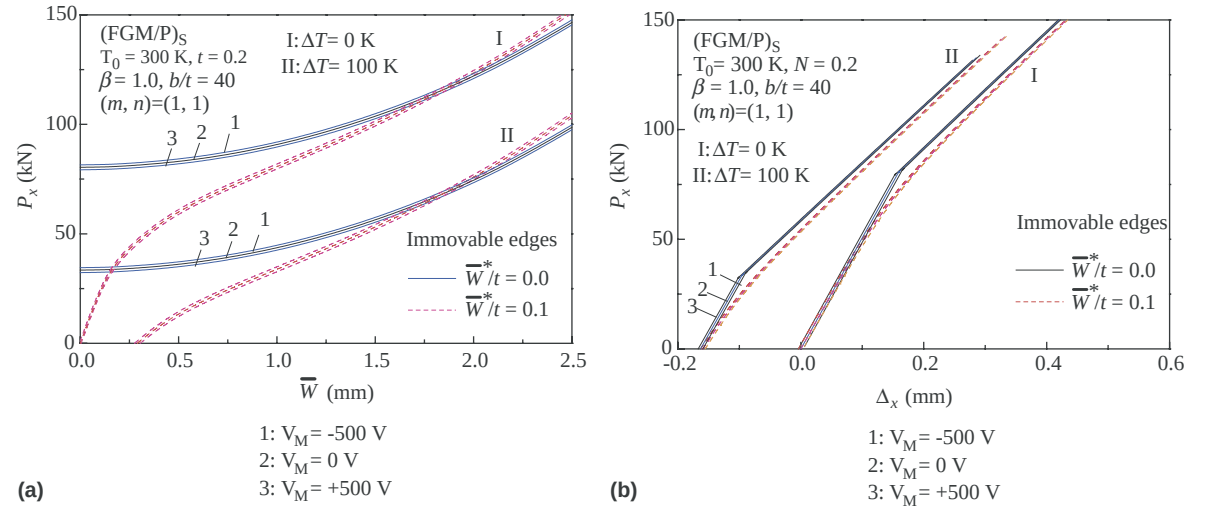

Fig. 4. Thermo-piezoelectric effects on the postbuckling behavior of $(FGM/P)_S$ plates with unload edges immovable. (a) Load–deflection (b) load–shortening.

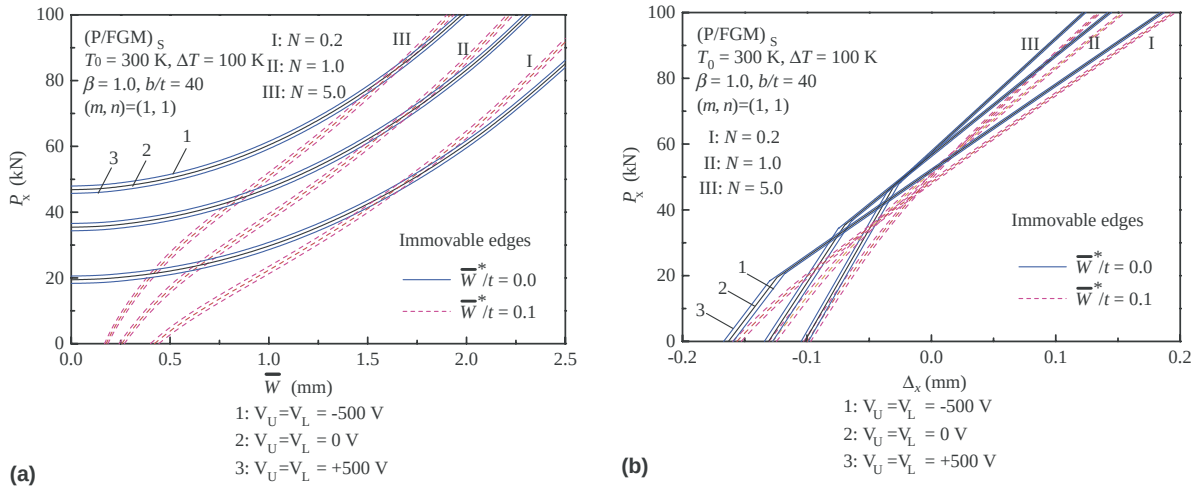

Fig. 5. Effects of volume fraction index N on the postbuckling behavior of $(P/FGM)_S$ plates with unload edges immovable. (a) Load–deflection (b) load–shortening.

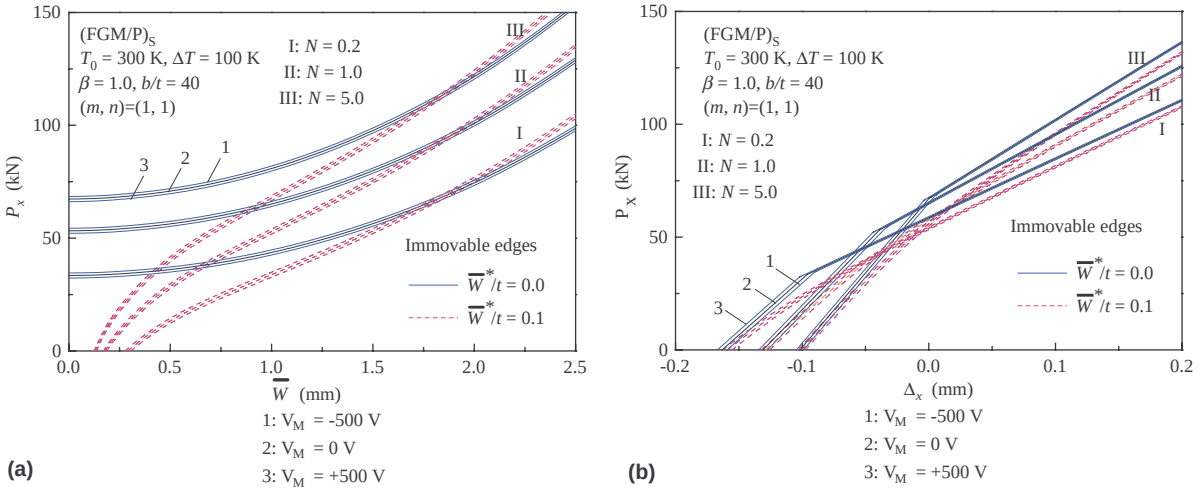

Fig. 6. Effects of volume fraction index N on the postbuckling behavior of $(FGM/P)_S$ plates with unload edges immovable. (a) Load–deflection, (b) load–shortening.

5. Concluding remarks

To study the effects of temperature dependency, temperature rise and control voltage on the postbuckling behavior of FGM hybrid laminated plates, a fully nonlinear postbuckling analysis has been presented. Numerical calculations have been made for mid-plane symmetric FGM plates with fully covered or embedded piezoelectric actuators under different sets of thermal and electrical loading conditions. The results show that the plate has lower buckling load and postbuckling paths when the temperature-dependent properties are taken into account. The results reveal that the temperature rise and the volume fraction distribution of FGMs layers have a significant effect on the buckling load and postbuckling behavior of FGM

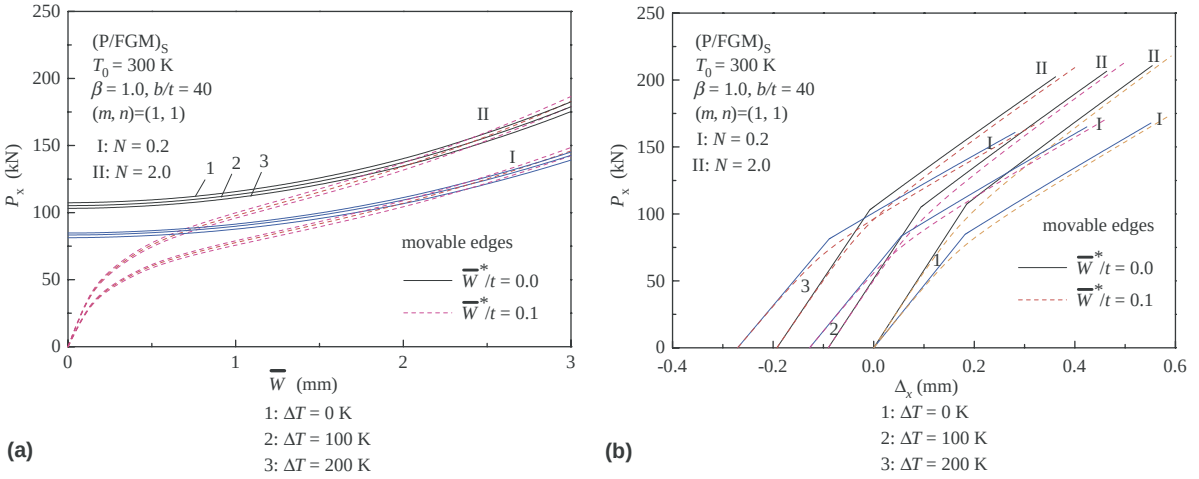

Fig. 7. Effects of temperature rise on the postbuckling behavior of $(P/FGM)_S$ plates with unload edges movable. (a) Load–deflection, (b) load–shortening.

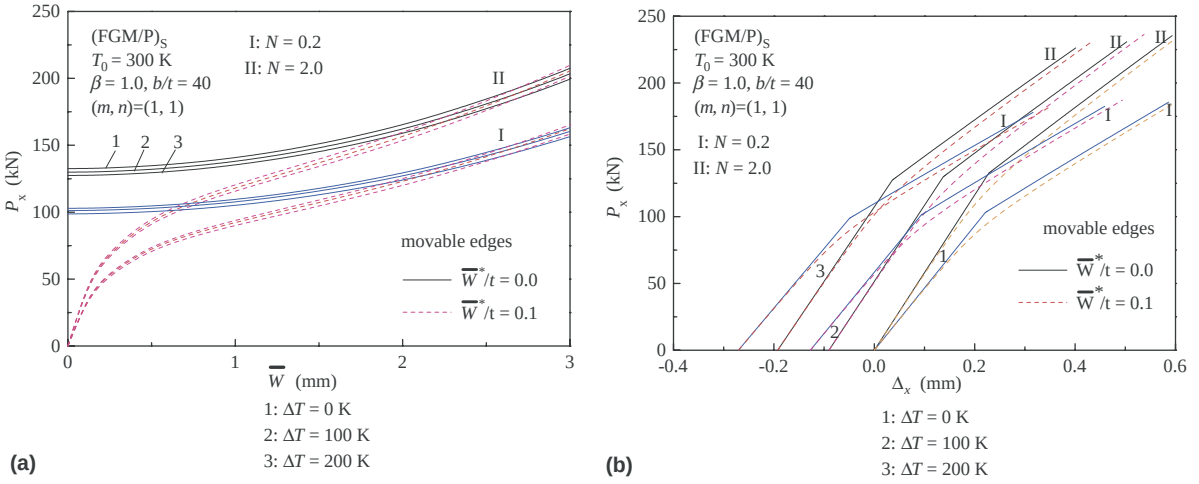

Fig. 8. Effects of temperature rise on the postbuckling behavior of $(FGM/P)_S$ plates with unload edges movable. (a) Load–deflection, (b) load–shortening.

hybrid laminated plates. In contrast, the control voltage only has a small effect on the buckling load and postbuckling behavior of FGM hybrid laminated plates with immovable unloaded edges, and it has almost no effect on the buckling load and postbuckling behavior of FGM hybrid laminated plates with movable unloaded edges. As a result, buckling control is hardly carried out for moderately thick hybrid laminated plates.

It is hoped that the results reported herein will contribute to a better understanding of the postbuckling behavior for FGM hybrid laminated plates under thermo-electro-mechanical loadings.

Acknowledgement

This work is supported in part by the National Natural Science Foundation of China under Grant 50375091. The author is grateful for this financial support.

Appendix A

In Eqs. (35) and (36)

$$(\lambda_x^{(0)},\lambda_x^{(2)},\lambda_x^{(4)})=\frac{1}{4\beta^2\gamma_{14}C_{11}}(S_0,S_2,S_4),\quad \delta_x^{(0)}=C_{00}\lambda_x-\delta_x^P,$$
$$\delta_x^{(2)}=\frac{1}{32\beta^2}C_{11}(1+2\mu),\quad \delta_x^{(4)}=\frac{1}{256\beta^2}\gamma_{14}\gamma_{24}C_{11}^2\left(\frac{m^4}{J_{13}\gamma_{24}^2}+\frac{n^4\beta^4}{J_{31}}\right)(1+\mu)^2(1+2\mu)^2 \tag{A.1}$$

in which (with g_{08}, g_{138} and g_{318} are defined as in Shen (2002))

$$S_0=\frac{\Theta_{11}}{(1+\mu)}-S_0^P,\quad S_2=\frac{1}{16}\gamma_{14}\gamma_{24}\Theta_2(1+2\mu),\quad S_4=\frac{1}{256}\gamma_{14}^2\gamma_{24}^2C_{11}(C_{24}-C_{44}),$$
$$\Theta_{11}=g_{08},\quad \Theta_{13}=g_{138},\quad \Theta_{31}=g_{318}$$
$$\Theta_2=\left(\frac{m^4}{\gamma_{24}^2}+n^4\beta^4+C_{22}\right),\quad C_{24}=2(1+\mu)^2(1+2\mu)^2\Theta_2\left(\frac{m^4}{J_{13}\gamma_{24}^2}+\frac{n^4\beta^4}{J_{31}}\right), \tag{A.2}$$
$$C_{44}=(1+\mu)(1+2\mu)\left[2(1+\mu)^2+(1+2\mu)\right]\left(\frac{m^8}{J_{13}\gamma_{24}^4}+\frac{n^8\beta^8}{J_{31}}\right)$$
$$J_{13}=\Theta_{13}C_{11}(1+\mu)-\Theta_{11}C_{13}+J^P,\quad J_{31}=\Theta_{31}C_{11}(1+\mu)-\Theta_{11}C_{31}-J^P$$

in the above equations, for the case of four edges movable

$$C_{00}=\gamma_{24},\quad C_{11}=C_{13}=m^2,\quad C_{31}=9m^2,\quad C_{22}=0,\quad S_0^P=J^P=0,$$
$$\delta_x^P=\frac{1}{4\beta^2\gamma_{24}}[(\gamma_{24}^2\gamma_{T1}-\gamma_5\gamma_{T2})\Delta T+(\gamma_{24}^2\gamma_{P1}-\gamma_5\gamma_{P2})\Delta V] \tag{A.3}$$

and for the case of unloaded edges immovable

$$C_{00}=\frac{1}{\gamma_{24}}(\gamma_{24}^2-\gamma_5^2)$$
$$C_{11}=m^2+\gamma_5n^2\beta^2,\quad C_{13}=m^2+9\gamma_5n^2\beta^2,\quad C_{31}=9m^2+\gamma_5n^2\beta^2,\quad C_{22}=2n^4\beta^4,$$
$$S_0^P=\gamma_{14}n^2\beta^2[(\gamma_{T2}-\gamma_5\gamma_{T1})\Delta T+(\gamma_{P2}-\gamma_5\gamma_{P1})\Delta V], \tag{A.4}$$
$$\delta_x^P=\frac{C_{00}}{4\beta^2}(\gamma_{T1}\Delta T+\gamma_{P1}\Delta V),$$
$$J^P=8\gamma_{14}m^2n^2\beta^2(1+\mu)[(\gamma_{T2}-\gamma_5\gamma_{T1})\Delta T+(\gamma_{P2}-\gamma_5\gamma_{P1})\Delta V].$$

References

Birman, V., 1995. Stability of functionally graded hybrid composite plates. Composites Engineering 5, 913–921.

Cui, E.J., Dowell, E.H., 1983. Postbuckling behavior of rectangular orthotropic plates with two free side edges. International Journal of Mechanical Sciences 25, 429–446.

Dym, C.L., 1974. Stability Theory and Its Applications to Structural Mechanics. Noordhoff, Leyden.
Feldman, E., Aboudi, J., 1997. Buckling analysis of functionally graded plates subjected to uniaxial loading. Composite Structures 38, 29–36.
Javaheri, R., Eslami, M.R., 2002a. Buckling of functionally graded plates under in-plane compressive loading. ZAMM 82, 277–283.
Javaheri, R., Eslami, M.R., 2002b. Thermal buckling of functionally graded plates. AIAA Journal 40, 162–169.
Javaheri, R., Eslami, M.R., 2002c. Thermal buckling of functionally graded plates based on higher order theory. Journal of Thermal Stresses 25, 603–625.
Leissa, A.W., 1986. Conditions for laminated plates to remain flat under inplane loading. Composite Structures 6, 261–270.
Librescu, L., Stein, M., 1991. A geometrically nonlinear theory of transversely isotropic laminated composite plates and its use in the post-buckling analysis. Thin-Walled Structures 11, 177–201.
Liew, K.M., Yang, J., Kitipornchai, S., 2003. Postbuckling of piezoelectric FGM plates subject to thermo-electro-mechanical loading. International Journal of Solids and Structures 40, 3869–3892.
Ma, L.S., Wang, T.J., 2003a. Nonlinear bending and post-buckling of a functionally graded circular plate under mechanical and thermal loadings. International Journal of Solids and Structures 40, 3311–3330.
Ma, L.S., Wang, T.J., 2003b. Axisymmetric post-buckling of a functionally graded circular plate subjected to uniformly distributed radial compression. Materials Science Forum 423–425, 719–724.
Najafizadeh, M.M., Eslami, M.R., 2002a. Buckling analysis of circular plates of functionally graded materials under uniform radial compression. International Journal of Mechanical Sciences 44, 2479–2493.
Najafizadeh, M.M., Eslami, M.R., 2002b. First-order-theory-based thermoelastic stability of functionally graded material circular plates. AIAA Journal 40, 1444–1450.
Oh, I.K., Han, J.H., Lee, I., 2000. Postbuckling and vibration characteristics of piezolaminated composite plate subjected to thermo-piezoelectric loads. Journal of Sound and Vibration 233, 19–40.
Qatu, M.S., Leissa, A.W., 1993. Buckling or transverse deflections of unsymmetrically laminated plates subjected to in-plane loads. AIAA Journal 31, 189–194.
Reddy, J.N., 1984a. A simple higher-order theory for laminated composite plates. Journal of Applied Mechanics ASME 51, 745–752.
Reddy, J.N., 1984b. A refined nonlinear theory of plates with transverse shear deformation. International Journal of Solids and Structures 20, 881–896.
Reddy, J.N., 1999. On laminated composite plates with integrated sensors and actuators. Engineering Structures 21, 568–593.
Reddy, J.N., Chin, C.D., 1998. Thermoelastical analysis of functionally graded cylinders and plates. Journal of Thermal Stresses 21, 593–626.
Shen, H.-S., 1998. Thermomechanical postbuckling analysis of imperfect laminated plates using a higher-order shear deformation theory. Computers and Structures 66, 395–409.
Shen, H.-S., 2000a. Postbuckling analysis of shear deformable laminated plates on two-parameter elastic foundations. Mechanics of Composite Materials and Structures 7, 249–268.
Shen, H.-S., 2000b. Thermomechanical postbuckling of imperfect shear deformable laminated plates on elastic foundations. Computer Methods in Applied Mechanics and Engineering 189, 761–784.
Shen, H.-S., 2000c. Postbuckling of shear deformable laminated plates under biaxial compression and lateral pressure and resting on elastic foundations. International Journal of Mechanical Sciences 42, 1171–1195.
Shen, H.-S., 2001. Postbuckling of shear deformable laminated plates with piezoelectric actuators under complex loading conditions. International Journal of Solids and Structures 38, 7703–7721.
Shen, H.-S., 2002. Nonlinear bending response of functionally graded plates subjected to transverse loads and in thermal environments. International Journal of Mechanical Sciences 44, 561–584.
Shen, H.-S., Zhang, J.-W., 1988. Perturbation analyses for the postbuckling of simply supported rectangular plates under uniaxial compression. Applied Mathematics and Mechanics 9, 793–804.
Touloukian, Y.S., 1967. Thermophysical Properties of High Temperature Solid Materials. Macmillan, New York.
Wu, L., 2004. Thermal buckling of simply supported moderately thick rectangular FGM plate. Composite Structures 64, 211–218.
Yamaki, N., 1961. Experiments on the postbuckling behavior of square plates loaded in edge compression. Journal of Applied Mechanics ASME 28, 238–244.
Yang, J., Shen, H.-S., 2003. Nonlinear analysis of functionally graded plates under transverse and in-plane loads. International Journal of Non-Linear Mechanics 38, 467–482.